



## Combined Upper Limits on Standard Model Higgs Boson Production from the DØ Experiment in up to $8.6 \text{ fb}^{-1}$ of Data

The DØ Collaboration  
URL <http://www-d0.fnal.gov>  
(Dated: July 24, 2011)

Searches for standard model Higgs boson production in  $p\bar{p}$  collisions at  $\sqrt{s} = 1.96 \text{ TeV}$  are carried out for Higgs boson masses ( $m_H$ ) in the range  $100 \leq m_H \leq 200 \text{ GeV}/c^2$ . The contributing production processes include gluon-gluon fusion ( $gg \rightarrow H$ ), associated production ( $q\bar{q} \rightarrow W/ZH$ ) and vector boson fusion ( $q\bar{q} \rightarrow q\bar{q}H$ ). Analyses are conducted in 40 distinct channels with integrated luminosities ranging from  $4.3$  to  $8.6 \text{ fb}^{-1}$ . As no significant excess is observed, we set limits on standard model Higgs boson production. The observed 95% C.L. upper limits are found to be a factor of 1.83 (0.71) times the predicted standard model cross section at  $m_H = 115$  (165)  $\text{GeV}/c^2$ , while the expected limit is found to be a factor of 1.90 (0.87) times the standard model prediction for the same mass. We exclude at the 95% C.L. the region  $161 < m_H < 170 \text{ GeV}/c^2$  with an *a priori* expected exclusion of  $159 < m_H < 170 \text{ GeV}/c^2$ .

*Preliminary Results for Summer 2011 Conferences*

## I. INTRODUCTION

Despite its success as a predictive tool, the standard model (SM) of particle physics remains incomplete without a means to explain electroweak symmetry breaking. The simplest proposed mechanism involves the introduction of a complex doublet of scalar fields that generate the masses of elementary particles via their mutual interactions. After accounting for longitudinal polarizations for the electroweak bosons, this so-called Higgs mechanism also gives rise to a single scalar boson with an unpredicted mass. Direct searches in  $e^+e^- \rightarrow Z^* \rightarrow ZH$  at the Large Electron Positron (LEP) collider yielded a lower mass limit at  $m_H > 114.4 \text{ GeV}/c^2$  [1] while precision electroweak data yield the indirect constraint  $m_H < 158 \text{ GeV}/c^2$  [2], with both limits set at 95% confidence level (C.L.). When also considering the direct limit, the indirect constraint predicts  $m_H < 185 \text{ GeV}/c^2$ , indicating that the range  $100 \leq m_H \leq 200 \text{ GeV}/c^2$  is the most important search region for a SM Higgs boson. The search for a SM Higgs boson is one of the main goals of the Fermilab Tevatron physics program.

In this note, we combine the results of direct searches for SM Higgs bosons in  $p\bar{p}$  collisions at  $\sqrt{s} = 1.96 \text{ TeV}$  recorded by the DØ experiment [3]. The analyses combined here seek signals of Higgs bosons produced through gluon-gluon fusion (GGF) ( $gg \rightarrow H$ ), in association with vector bosons ( $q\bar{q} \rightarrow VH$  where  $V = W, Z$ ) and through vector boson fusion (VBF) ( $q\bar{q} \rightarrow q\bar{q}H$ ). The analyses utilize data corresponding to integrated luminosities ranging from 4.3 to 8.6  $\text{fb}^{-1}$ , collected during the data taking period 2002-2011. The Higgs boson decay modes studied are  $H \rightarrow b\bar{b}$ ,  $H \rightarrow W^+W^-$ ,  $H \rightarrow \tau^+\tau^-$  and  $H \rightarrow \gamma\gamma$ . The searches are organized into 40 analysis sub-channels comprising different production, decay and final state particle configurations, each designed to maximize the sensitivity for a particular Higgs boson production and decay mode. In order to facilitate proper combination of signals, the analyses were constructed to be mutually exclusive after analysis selections. Searches for several final states are further divided into distinct epochs of data collection and reconstruction. The most notable divide is between data collected before and after the 2006 DØ detector upgrade. The largest changes made during the upgrade were the addition of a new layer to the silicon detector nearest to the beam-line and an upgrade of the trigger system. The two epochs are denoted as Run IIa (1.1  $\text{fb}^{-1}$ ) and Run IIb (on-going, currently up to 7.5  $\text{fb}^{-1}$  are analyzed in this note). Some analyses have also divided the Run IIb data epoch into two smaller parts differentiated primarily by a change to the vertex reconstruction algorithm.

The analyses used in this combination [4–12] are outlined in Table I. In the cases of  $p\bar{p} \rightarrow (W/Z)H$  production, we search for a Higgs boson decaying to two bottom quarks, or two tau leptons. The decays of the vector bosons further define the analyzed final states. To isolate  $H \rightarrow b\bar{b}$  decays, an algorithm for identifying jets consistent with the decay of a heavy-flavor quark is applied to each jet ( $b$ -tagging). Several kinematic variables sensitive to displaced jet vertices and jet tracks with large transverse impact parameters relative to the hard-scatter vertices are combined in a new boosted decision tree based  $b$ -tagging discriminant. The new algorithm is an upgraded version of the neural network  $b$ -tagger used previously [13]. By adjusting a minimum requirement on the  $b$ -tagging output a spectrum of increasingly stringent  $b$ -tagging operating points is achieved, each with a different signal efficiency and purity. For the  $WH \rightarrow \ell\nu b\bar{b}$ ,  $ZH \rightarrow \nu\bar{\nu} b\bar{b}$  and  $ZH \rightarrow \ell\ell b\bar{b}$  processes, the analyses are separated into two groups: one in which two of the jets are  $b$ -tagged with a loose tag requirement ( $WH \rightarrow \ell\nu b\bar{b}$  and  $ZH \rightarrow \nu\bar{\nu} b\bar{b}$ ) or one loose and one tight tag requirement ( $ZH \rightarrow \ell\ell b\bar{b}$ ) (double  $b$ -tag or DT) and an orthogonal group in which only one jet has a loose ( $WH \rightarrow \ell\nu b\bar{b}$  and  $ZH \rightarrow \nu\bar{\nu} b\bar{b}$ ) or tight ( $ZH \rightarrow \ell\ell b\bar{b}$ )  $b$ -tag (single  $b$ -tag or ST). A typical per-jet efficiency and fake rate for the loose (tight)  $b$ -tag selection is about 80% (50%) and 10% (0.5%), respectively. Furthermore, the  $WH \rightarrow \ell\nu b\bar{b}$  and  $ZH \rightarrow \nu\bar{\nu} b\bar{b}$  analyses use the output from the  $b$ -tagger as input to final discriminants. For all three analyses, each lepton flavor of the  $W/Z$  boson decay ( $\ell = e, \mu$ ) is treated as an independent channel. The  $ZH \rightarrow \nu\bar{\nu} b\bar{b}$  analysis includes the signal contribution from  $WH \rightarrow \ell\nu b\bar{b}$  production where the primary lepton from the  $W$  boson decay falls outside of the detector fiducial volume or is not identified as a lepton.

We also consider Higgs decays to two  $W^\pm$  bosons for the three dominant production mechanisms: gluon-gluon fusion, associated production and vector-boson fusion. In the case of production via gluon-gluon fusion and vector-boson fusion, we search for leptonic  $W$  boson decays with five final states of opposite-signed leptons:  $WW \rightarrow e^+\nu e^-\nu$ ,  $e^\pm\nu\mu^\mp\nu$ ,  $\mu^+\nu\mu^-\nu$ ,  $e^\pm\nu\tau_{had}^\mp\nu$  and  $\mu^\pm\nu\tau_{had}^\mp\nu$ , where  $\tau_{had}$  denotes a hadronic tau decay. In addition we consider final states originating from Higgs boson production in association with a vector boson ( $WH$  or  $ZH$ ), where leptons may originate from the vector boson or Higgs boson decay. We classify events according to their jet multiplicity in order to isolate particular signal production mechanisms and optimize the discrimination between signal and background. The  $H \rightarrow W^+W^- \rightarrow \ell^\pm\nu\ell^\mp\nu$  ( $\ell = e, \mu$ ) analyses further separate events in three final states with 0 jets, 1 jet, and 2 or more jets. Analyses identifying hadronic tau candidates select events with  $\leq 1$  jets, mainly sensitive to the gluon-gluon fusion signal, or with  $\geq 2$  jets, also sensitive to associated production and vector-boson fusion. At high mass, the dominant signal contribution to both tau analyses originates from  $H \rightarrow W^+W^- \rightarrow \mu^\pm\nu\tau^\mp\nu$ . The tau analyses requiring at least two jets select significant signal at low mass from  $ZH \rightarrow \tau\tau b\bar{b}$  and  $W/ZH \rightarrow q\bar{q}\tau\tau$ . Another analysis considers the semileptonic decay  $H \rightarrow W^+W^- \rightarrow \ell\nu q\bar{q}$ . In all  $H \rightarrow W^+W^-$  decays with  $m_H < 2m_W$ , at least one of the  $W$  bosons will be off mass shell. For  $VH \rightarrow \ell^\pm\ell^\pm + X$  production, we search for leptonic  $W$  boson decays with three final states of same-signed leptons:  $VWW \rightarrow e^\pm\nu e^\pm\nu + X$ ,  $e^\pm\nu\mu^\pm\nu + X$ , and  $\mu^\pm\nu\mu^\pm\nu + X$ . Finally, we

include an analysis that searches for Higgs bosons decaying to two photons and produced via gluon-gluon fusion, vector boson fusion, and associated production mechanisms.

Since the last DØ SM combined Higgs boson search over the this full mass range [14, 15], we have updated the  $WH \rightarrow \ell\nu b\bar{b}$ ,  $ZH \rightarrow \nu\bar{\nu} b\bar{b}$ ,  $ZH \rightarrow \ell\bar{\ell} b\bar{b}$ ,  $H \rightarrow W^+W^- \rightarrow \ell^\pm \nu \ell^\mp \nu$ ,  $H \rightarrow W^+W^- \rightarrow \ell\nu q\bar{q}$ ,  $H+X \rightarrow \ell^\pm \tau_{had}^\mp jj$  and  $H \rightarrow \gamma\gamma$  analyses. This is the first time including the  $H+X \rightarrow \mu^\pm \tau_{had}^\mp + \leq 1j$  channel in this full mass combination.

TABLE I: List of analysis channels, corresponding integrated luminosities, and final variables used for setting limits, which is either a decision-tree (DTree) or neural-network (NN) discriminant. See Sect. I for details ( $\ell = e, \mu$ ).

Channel	Luminosity (fb <sup>-1</sup> )	Final Variable	# Sub-Channels	Data Epochs	Reference
$WH \rightarrow \ell\nu b\bar{b}$ , ST/DT, 2/3 jet	8.5	DTree discriminant	8	3	[4]
$ZH \rightarrow \nu\bar{\nu} b\bar{b}$ , ST/DT	8.4	DTree discriminant	2	3	[5]
$ZH \rightarrow \ell\bar{\ell} b\bar{b}$ , ST/DT	8.6	DTree discriminant	10	3	[6]
$H \rightarrow W^+W^- \rightarrow \ell^\pm \nu \ell^\mp \nu$ , 0/1/2+ jet	8.1	DTree discriminant	9	2	[7]
$H \rightarrow W^+W^- \rightarrow \ell\nu q\bar{q}$	5.4	DTree discriminant	2	2	[8]
$H+X \rightarrow \mu^\pm \tau_{had}^\mp + \leq 1j$	7.3	NN discriminant	3	1	[9]
$VH \rightarrow \ell^\pm \ell^\pm + X$	5.3	DTree discriminant	3	2	[10]
$H+X \rightarrow \ell^\pm \tau_{had}^\mp jj$	4.3	DTree discriminant	2	1	[11]
$H \rightarrow \gamma\gamma$	8.2	DTree discriminant	1	1	[12]

The backgrounds from multijet production are measured in data. The other backgrounds were generated by PYTHIA [16], ALPGEN [17], and COMPHEP [18], with PYTHIA providing parton-showering and hadronization. Background cross sections are normalized either to next-to-leading order (NLO) calculations from MCFM [19] or, whenever possible, to data control samples.

## II. SIGNAL PREDICTIONS AND UNCERTAINTIES

A common approach to the signal predictions and associated uncertainties is followed by the CDF and DØ Collaborations. An outline of the procedures followed is given here; more complete discussion can be found in Ref. [20].

The Monte Carlo signal simulation is provided by the LO generator PYTHIA (with CTEQ5L and CTEQ6L1 [38] leading-order (LO) parton distribution functions) which includes a parton shower and fragmentation and hadronization models. We reweight the Higgs boson  $p_T$  spectra in our PYTHIA Monte Carlo samples to that predicted by HQT [39] when making predictions of differential distributions of GGF signal events. To evaluate the impact of the scale uncertainty on our differential spectra, we use the RESBOS [40] generator, and apply the scale-dependent differences in the Higgs boson  $p_T$  spectrum to the HQT prediction, and propagate these to our final discriminants as a systematic uncertainty on the shape, which is included in the calculation of the limits.

We normalize our Higgs boson signal predictions to the most recent high-order calculations available. The  $gg \rightarrow H$  production cross section we use is calculated at next-to-next-to leading order (NNLO) in QCD with a next-to-next-to leading log (NNLL) resummation of soft gluons; the calculation also includes two-loop electroweak effects and handling of the running  $b$  quark mass [21, 22]. The numerical values in Table II are updates [23] of these predictions with  $m_t$  set to 173.1 GeV/ $c^2$  [24], and an exact treatment of the massive top and bottom loop corrections up to NLO + next-to-leading-log accuracy. The factorization and renormalization scale choice for this calculation is  $\mu_F = \mu_R = m_H$ . These calculations are refinements of the earlier NNLO calculations of the  $gg \rightarrow H$  production cross section [26–28]. Electroweak corrections were computed in Refs. [29, 30]. Soft gluon resummation was introduced in the prediction of the  $gg \rightarrow H$  production cross section in Ref. [31]. The  $gg \rightarrow H$  production cross section depends strongly on the gluon parton density function, and the accompanying value of  $\alpha_s(q^2)$ . The cross sections used here are calculated with the MSTW 2008 NNLO PDF set [32], as recommended by the PDF4LHC working group [33]. The inclusive Higgs boson production cross sections are listed in Table II.

For analyses that consider inclusive  $gg \rightarrow H$  production but do not split it into separate channels based on the number of reconstructed jets, we use the inclusive uncertainties from the simultaneous variation of the factorization and renormalization scale up and down by a factor of two. We use the prescription of the PDF4LHC working group for evaluating PDF uncertainties on the inclusive production cross section. QCD scale uncertainties that affect the cross section via their impacts on the PDFs are included as a correlated part of the total scale uncertainty. The remainder of the PDF uncertainty is treated as uncorrelated with the QCD scale uncertainty.

For analyses seeking  $gg \rightarrow H$  production that divide events into categories based on the number of reconstructed jets, we employ a new approach for evaluating the impacts of the scale uncertainties. Following the recommendations

TABLE II: The production cross sections (in fb) and decay branching fractions (in %) for each SM Higgs boson mass (in GeV/ $c^2$ ) assumed for the combination.

$m_H$	$\sigma_{gg \rightarrow H}$	$\sigma_{WH}$	$\sigma_{ZH}$	$\sigma_{VBF}$	$B(H \rightarrow b\bar{b})$	$B(H \rightarrow c\bar{c})$	$B(H \rightarrow \tau^+\tau^-)$	$B(H \rightarrow W^+W^-)$	$B(H \rightarrow ZZ)$	$B(H \rightarrow \gamma\gamma)$
100	1821.8	291.90	169.8	100.1	79.1	3.68	8.36	1.11	0.113	0.159
105	1584.7	248.40	145.9	92.3	77.3	3.59	8.25	2.43	0.215	0.178
110	1385.0	212.00	125.7	85.1	74.5	3.46	8.03	4.82	0.439	0.197
115	1215.9	174.50	103.9	78.6	70.5	3.27	7.65	8.67	0.873	0.213
120	1072.3	150.10	90.2	72.7	64.9	3.01	7.11	14.3	1.60	0.225
125	949.3	129.50	78.5	67.1	57.8	2.68	6.37	21.6	2.67	0.230
130	842.9	112.00	68.5	62.1	49.4	2.29	5.49	30.5	4.02	0.226
135	750.8	97.20	60.0	57.5	40.4	1.87	4.52	40.3	5.51	0.214
140	670.6	84.60	52.7	53.2	31.4	1.46	3.54	50.4	6.92	0.194
145	600.6	73.70	46.3	49.4	23.1	1.07	2.62	60.3	7.96	0.168
150	539.1	64.40	40.8	45.8	15.7	0.725	1.79	69.9	8.28	0.137
155	484.0	56.20	35.9	42.4	9.18	0.425	1.06	79.6	7.36	0.100
160	432.3	48.50	31.4	39.4	3.44	0.159	0.397	90.9	4.16	0.0533
165	383.7	43.60	28.4	36.6	1.19	0.0549	0.138	96.0	2.22	0.0230
170	344.0	38.50	25.3	34.0	0.787	0.0364	0.0920	96.5	2.36	0.0158
175	309.7	34.00	22.5	31.6	0.612	0.0283	0.0719	95.8	3.23	0.0123
180	279.2	30.10	20.0	29.4	0.497	0.0230	0.0587	93.2	6.02	0.0102
185	252.1	26.90	17.9	27.3	0.385	0.0178	0.0457	84.4	15.0	0.00809
190	228.0	24.00	16.1	25.4	0.315	0.0146	0.0376	78.6	20.9	0.00674
195	207.2	21.40	14.4	23.7	0.270	0.0125	0.0324	75.7	23.9	0.00589
200	189.1	19.10	13.0	22.0	0.238	0.0110	0.0287	74.1	25.6	0.00526

of Ref. [25], we treat the QCD scale uncertainties obtained from the NNLL inclusive [21, 22], NLO one or more jets [36], and NLO two or more jets [37] cross section calculations as uncorrelated with one another. We then obtain QCD scale uncertainties for the exclusive  $gg \rightarrow H + 0$  jet, 1 jet, and 2 or more jet categories by propagating the uncertainties on the inclusive cross section predictions through the subtractions needed to predict the exclusive rates. For example, the  $H+0$  jet cross section is obtained by subtracting the NLO  $H + 1$  or more jet cross section from the inclusive NNLL+NNLO cross section. We now assign three separate, uncorrelated scale uncertainties which lead to correlated and anticorrelated uncertainty contributions between exclusive jet categories. The procedure in Ref. [36] is used to determine PDF model uncertainties. These are obtained separately for each jet bin and treated as 100% correlated between jet bins.

Another source of uncertainty in the prediction of  $\sigma(gg \rightarrow H)$  is the extrapolation of the QCD corrections computed for the heavy top quark loops to the light-quark loops included as part of the electroweak corrections. Uncertainties at the level of 1-2% are already included in the cross section values we use [21, 22]. In Ref. [21], it is argued that the factorization of QCD corrections is known to work well for Higgs boson masses many times in excess of the masses of the loop particles. A 4% change in the predicted cross section is seen when all QCD corrections are removed from the diagrams containing light-flavored quark loops, which is too conservative. For the  $b$  quark loop, which is computed separately in Ref. [21], the QCD corrections are much smaller than for the top loop, further giving confidence that it does not introduce large uncertainties.

We include all significant Higgs production modes in our searches. Besides GGF through virtual quark loops, we include Higgs boson production in association with a  $W$  or  $Z$  vector boson, and vector boson fusion. We use the  $WH$  and  $ZH$  production cross sections computed at NNLO [41]. This calculation starts with the NLO calculation of v2HV [42] and includes NNLO QCD contributions [43], as well as one-loop electroweak corrections [44]. We use the VBF cross section computed at NNLO in QCD [45]. Electroweak corrections to the VBF production cross section are computed with the HAWK program [46], and are very small (0.03 fb and less) for the Higgs boson mass range considered here.

The Higgs boson decay branching ratio predictions are calculated with HDECAY [47], and are also listed in Table II. We use HDECAY Version 3.53. While the  $HWW$  coupling is well predicted,  $B(H \rightarrow W^+W^-)$  depends on the partial widths of all other Higgs boson decays. The partial width  $\Gamma(H \rightarrow b\bar{b})$  is sensitive to  $m_b$  and  $\alpha_s$ ,  $\Gamma(H \rightarrow c\bar{c})$  is sensitive to  $m_c$  and  $\alpha_s$ , and  $\Gamma(H \rightarrow gg)$  is sensitive to  $\alpha_s$ . The impacts of these uncertainties on  $B(H \rightarrow W^+W^-)$  depend on  $m_H$  due to the fact that  $B(H \rightarrow b\bar{b})$ ,  $B(H \rightarrow c\bar{c})$ ,  $B(H \rightarrow gg)$  become very small for Higgs boson masses above 160 GeV/ $c^2$ , while they have a larger impact for lower  $m_H$ . We use the uncertainties on the branching fraction  $B(H \rightarrow W^+W^-)$  from Ref. [48]. At  $m_H = 130$  GeV/ $c^2$ , for example, the  $m_b$  variation gives a  ${}_{+1.70}^{-4.89}\%$  relative variation in  $B(H \rightarrow W^+W^-)$ ,  $\alpha_s$  gives a  ${}_{+1.09}^{-1.02}\%$  variation, and  $m_c$  gives a  ${}_{+0.51}^{-0.45}\%$  variation. At  $m_H = 165$  GeV/ $c^2$ , all three of these uncertainties drop below 0.1%.

### III. LIMIT CALCULATIONS

We combine results using the  $CL_s$  method with a negative log-likelihood ratio (LLR) test statistic [49]. The value of  $CL_s$  is defined as  $CL_s = CL_{s+b}/CL_b$  where  $CL_{s+b}$  and  $CL_b$  are the confidence levels for the signal-plus-background hypothesis and the background-only hypothesis, respectively. These confidence levels are evaluated by integrating corresponding LLR distributions populated by simulating outcomes via Poisson statistics. Separate channels and bins are combined by summing LLR values over all bins and channels. This method provides a robust means of combining individual channels while maintaining individual channel sensitivities and incorporating systematic uncertainties. Systematics are treated as Gaussian uncertainties on the expected number of signal and background events, not the outcomes of the limit calculations. This approach ensures that the uncertainties and their correlations are propagated to the outcome with their proper weights. The  $CL_s$  approach used in this combination utilizes binned final-variable distributions rather than a single-bin (fully integrated) value for each contributing analysis. The exclusion criteria are determined by increasing the signal cross section until  $CL_s = 1 - \alpha$ , which defines a signal cross section excluded at 95% confidence level for  $\alpha = 0.95$ .

#### A. Final Variable Preparation

The final variables for all analyses (See Table I) are shown in Figs. 1-7. In several of these figures, multiple contributing sub-processes of common sources are summed together. All analyses are performed on a Higgs boson mass grid with steps of 5 GeV/ $c^2$ .

#### B. Systematic Uncertainties

The systematic uncertainties differ between analyses for both the signals and backgrounds [4–12]. Here we summarize only the largest contributions. Most analyses carry an uncertainty on the integrated luminosity of 6.1% [50], while the overall normalization of other analyses is determined from the NNLO  $Z/\gamma^*$  cross section in data events near the peak of  $Z \rightarrow \ell\ell$  decays. The  $H \rightarrow b\bar{b}$  analyses have an uncertainty on the  $b$ -tagging rate of 1-10%. These analyses also have an uncertainty on the jet measurement and acceptances of  $\sim 7\%$ . All analyses include uncertainties associated with lepton measurement and acceptances, which range from 1-9% depending on the final state. The largest contribution for all analyses is the uncertainty on the background cross sections at 4-30% depending on the analysis channel and specific background. These values include both the uncertainty on the theoretical cross section calculations and the uncertainties on the higher order correction factors. The uncertainty on the expected multijet background is dominated by the statistics of the data sample from which it is estimated, and is considered separately from the other cross section uncertainties. The  $H \rightarrow \gamma\gamma$  and  $H \rightarrow W^+W^- \rightarrow \ell\nu q\bar{q}$  analyses also assign two uncertainties to the NNLO gluon-gluon fusion Higgs production cross section associated with the accuracy of the inclusive cross section calculation due to PDF model and scale choice. The  $H \rightarrow W^+W^- \rightarrow \ell^+\nu\ell^-\nu$  ( $\ell = e, \mu$ ) analyses divide the data by jet multiplicity and, as discussed, apply different uncertainties for each jet multiplicity final state. In addition, several analyses incorporate shape-dependent uncertainties on the kinematics of the dominant backgrounds in the analyses. These shapes are derived from the potential variations of the final variables due to generator and background modeling uncertainties. Further details on the systematic uncertainties are given in Tables III-XI.

The systematic uncertainties for background rates are generally several times larger than the signal expectation itself and are an important factor in the calculation of limits. Each systematic uncertainty is folded into the signal and background expectations in the limit calculation via Gaussian distributions. These Gaussian values are sampled for each MC trial (pseudo-experiment) using Poisson distributions for the number of signal and background events. Several of the systematic uncertainties, for example the jet energy scale uncertainty, typically impact the shape of the final variable. These shape dependences were preserved in the description of systematic fluctuations for each Poisson trial. Correlations between systematic sources are carried through in the calculation. For example, the uncertainty on the integrated luminosity is held to be correlated between all signals and backgrounds and, thus, the same fluctuation in the luminosity is common to all channels for a single pseudo-experiment. All systematic uncertainties originating from a common source are held to be correlated, as detailed in Table XII.

To minimize the degrading effects of systematics on the search sensitivity, the individual background contributions are fitted to the data observation by maximizing a likelihood function for each hypothesis [51]. The likelihood is a joint Poisson probability over the number of bins in the calculation and is a function of the nuisance parameters in the system and their associated uncertainties, which are given an additional Gaussian constraint associated with their prior predictions. The maximization of the likelihood function is performed over the nuisance parameters. A fit is

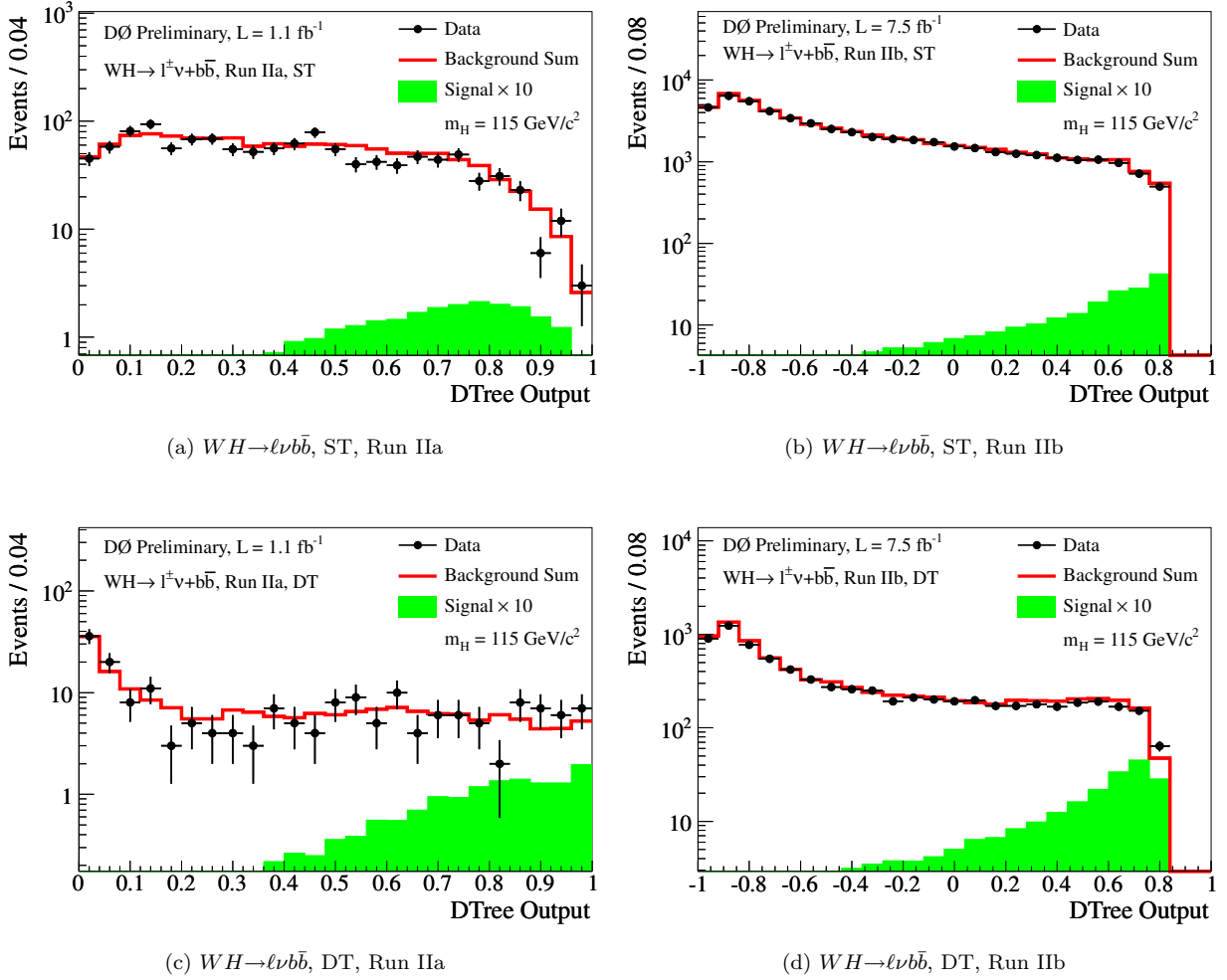


FIG. 1: Final variable distribution for the  $WH \rightarrow \ell \nu b \bar{b}$  analysis in (a) Run Ila ST, (b) Run Iib ST, (c) RunIla DT, and (d) Run Iib DT samples combined for 2 and 3 jets.

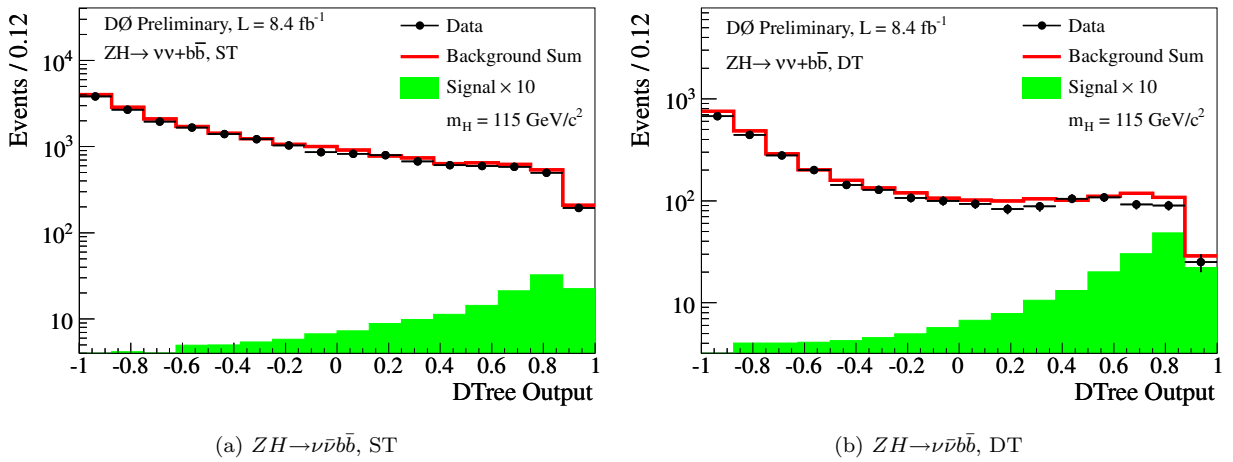


FIG. 2: Final variable distribution for the  $ZH \rightarrow \nu \bar{\nu} b \bar{b}$  analyses in (a) ST and (b) DT samples combined over all lepton channels and data periods.

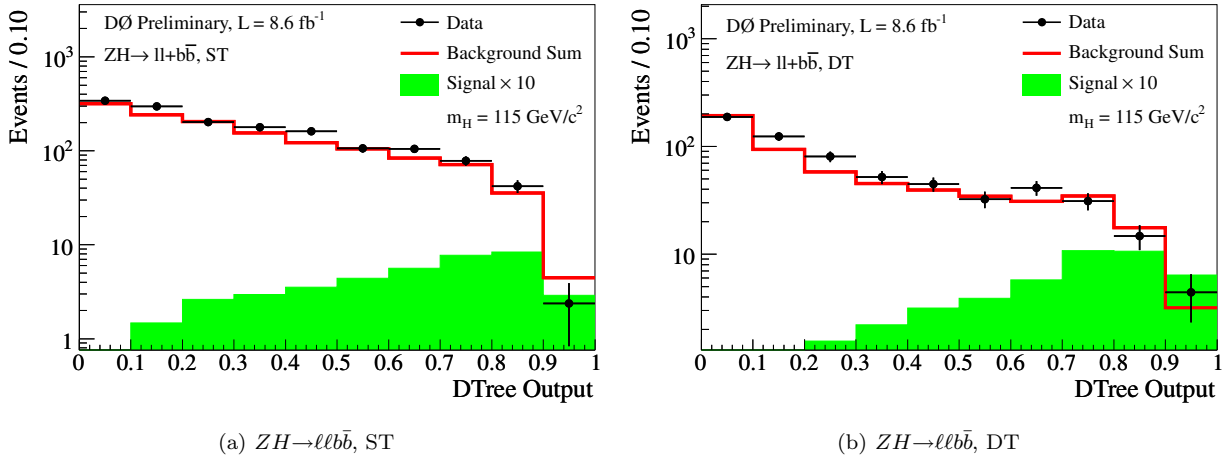


FIG. 3: Final variable distribution for the  $ZH \rightarrow \ell\ell b\bar{b}$  analyses in (a) ST and (b) DT samples combined over data periods.

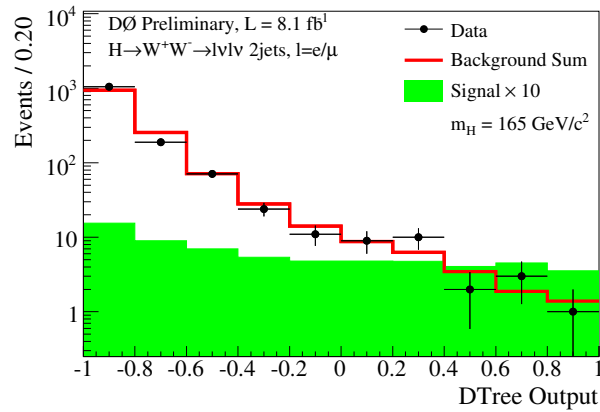
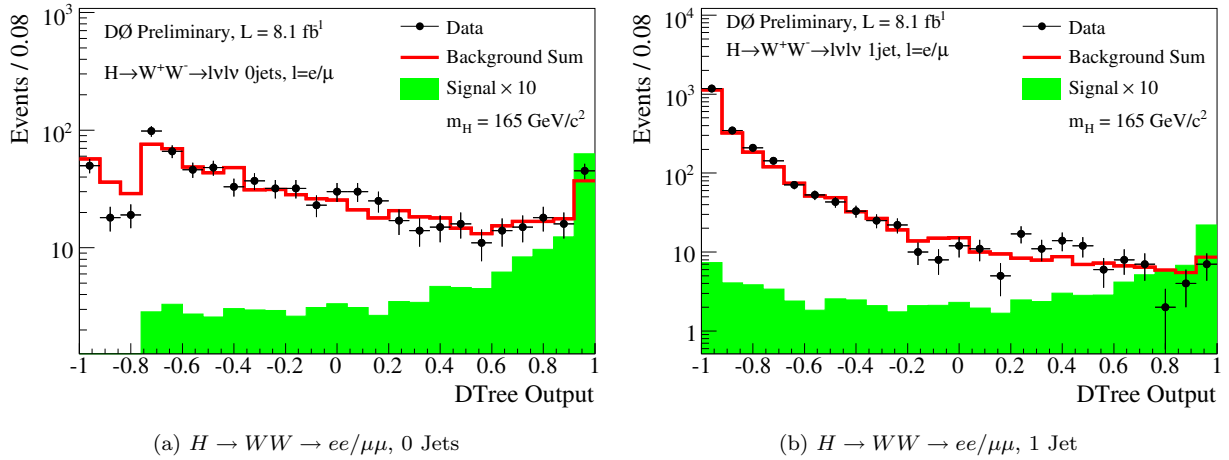


FIG. 4: Final variable distribution for the  $H \rightarrow WW \rightarrow ee/\mu\mu$  analysis in the 0,1, and 2 jets sub-channels combined over data periods.

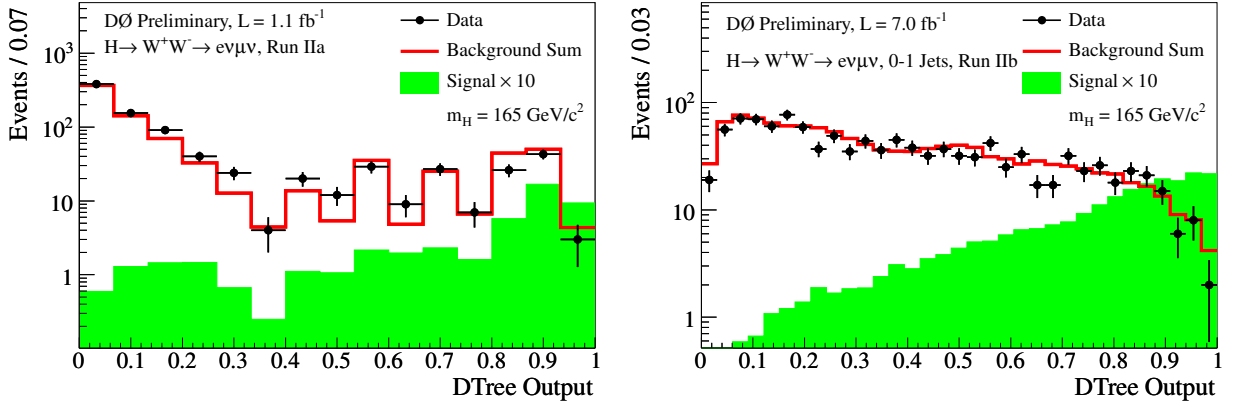
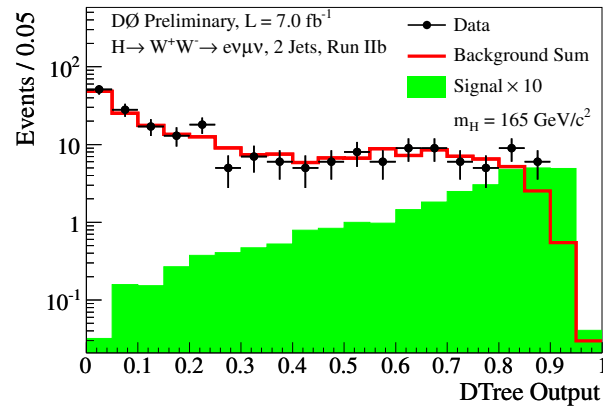
(a)  $H \rightarrow WW \rightarrow e\mu$ , Run IIA(b)  $H \rightarrow WW \rightarrow e\mu$ , 0-1 Jets, Run IIB(c)  $H \rightarrow WW \rightarrow e\mu$ , 2 Jets, Run IIB

FIG. 5: Final variable distribution for the  $H \rightarrow WW \rightarrow e\mu$  analysis in (a) the Run IIA period combined over 0, 1, and 2 jets sub-channels, (b) the Run IIB period combined over 0 and 1 jets sub-channels, and (c) the Run IIB period 2 jets sub-channel.

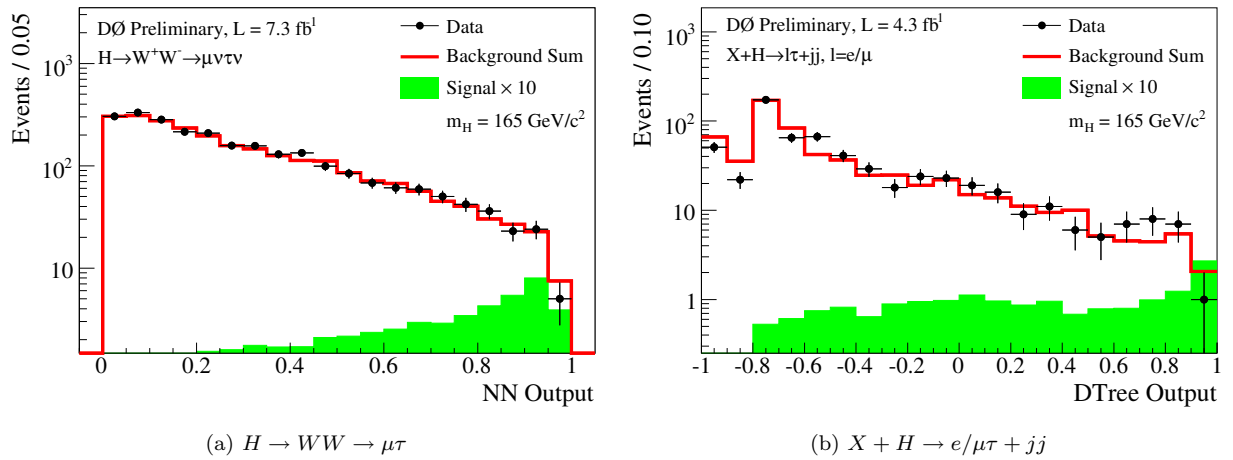
(a)  $H \rightarrow WW \rightarrow \mu\tau$ (b)  $X + H \rightarrow e/\mu\tau + jj$ 

FIG. 6: Final variable distribution for (a) the  $H \rightarrow WW \rightarrow \mu\tau$  analysis and (b) the  $X + H \rightarrow e/\mu\tau + jj$  analysis.

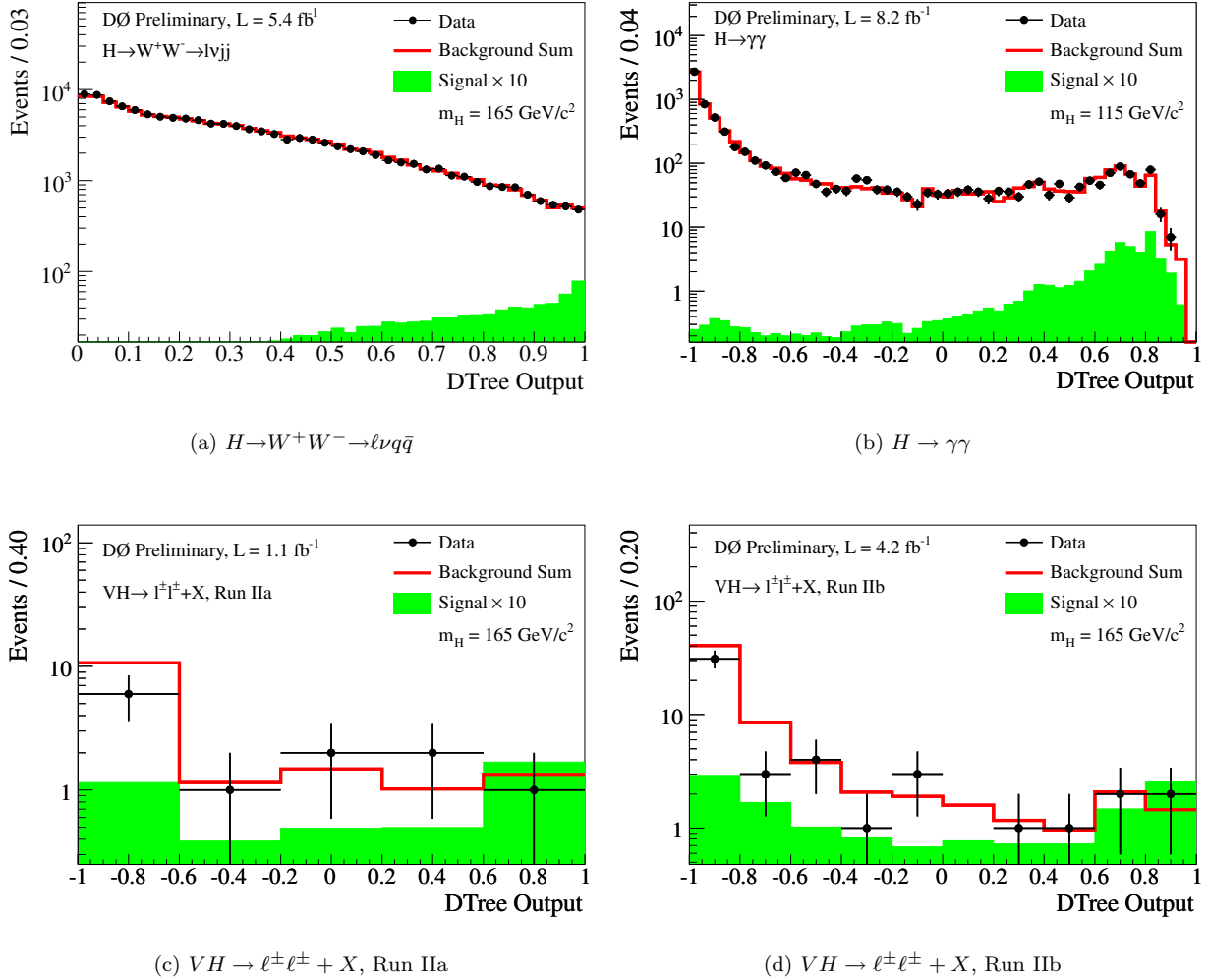


FIG. 7: Final variable distribution for (a) the  $H \rightarrow W^+ W^- \rightarrow \ell \nu q \bar{q}$  analysis combined over all sub-channels, (b) the  $H \rightarrow \gamma \gamma$  analysis, (c) the  $VH \rightarrow \ell^\pm \ell^\pm + X$  analysis for Run IIa combined over all lepton channels, and (d) the  $VH \rightarrow \ell^\pm \ell^\pm + X$  analysis for Run IIb combined over all lepton channels.

performed to both the background-only (b) and signal-plus-background (s+b) hypothesis separately for each Poisson MC trial.

#### IV. RESULTS

We derive limits, at 95% C.L., on SM Higgs boson production  $\sigma \times BR(H \rightarrow b\bar{b}/W^+W^-/\tau^+\tau^-/\gamma\gamma)$  via 40 individual channels [4–12]. To facilitate model transparency and to accommodate analyses with different degrees of sensitivity, we present our results in terms of the ratio of 95% C.L. upper cross section limits to the SM predicted cross section as a function of Higgs boson mass. The SM prediction for Higgs boson production would therefore be considered excluded at 95% C.L. when this limit ratio falls below unity.

The individual analyses described in Table I are grouped to evaluate combined limits over the range  $100 \leq M_H \leq 200 \text{ GeV}/c^2$ . The  $H+X \rightarrow \ell^\pm \tau_{had}^\mp jj$  analysis contributes to the region  $M_H \geq 105 \text{ GeV}/c^2$ , the  $ZH \rightarrow \ell\ell b\bar{b}$   $ZH \rightarrow \nu\bar{\nu} b\bar{b}$   $WH \rightarrow \ell\nu b\bar{b}$  and  $H \rightarrow \gamma\gamma$  analyses contribute for  $M_H \leq 150 \text{ GeV}/c^2$ , the  $VH \rightarrow \ell^\pm \ell^\pm + X$  analyses contribute for  $M_H \geq 115 \text{ GeV}/c^2$ , and the  $H \rightarrow W^+ W^- \rightarrow \ell\nu q\bar{q}$  analyses contribute for  $M_H \geq 155 \text{ GeV}/c^2$ .

Figure 8 shows the expected and observed 95% C.L. cross section limits as a ratio to the SM cross section and for the probed mass region ( $100 \leq m_H \leq 200 \text{ GeV}/c^2$ ), with all analyses combined. These results are also summarized

TABLE III: Systematic uncertainties on the signal and background contributions for the  $WH \rightarrow \ell\nu b\bar{b}$  single (ST) and double tag (DT) channels. Systematic uncertainties are listed by name, see the original references for a detailed explanation of their meaning and on how they are derived. Systematic uncertainties for  $WH$  shown in this table are obtained for  $m_H = 115$  GeV/ $c^2$ . Uncertainties are relative, in percent, and are symmetric unless otherwise indicated. Shape uncertainties are labeled with an “(S)”, and “SH” represents shape only uncertainty.

$WH \rightarrow \ell\nu b\bar{b}$  Single Tag (ST) channels relative uncertainties (%)

Contribution	Dibosons	$W + b\bar{b}/c\bar{c}$	$W+l.f.$	$t\bar{t}$	single top	Multijet	$WH$
Luminosity	6.1	6.1	6.1	6.1	6.1	–	6.1
Electron ID/Trigger eff. (S)	1–5	2–4	2–4	1–2	1–2	–	2–3
Muon Trigger eff. (S)	1–3	1–2	1–3	2–5	2–3	–	2–4
Muon ID/Reco eff./resol.	4.1	4.1	4.1	4.1	4.1	–	4.1
Jet ID/Reco eff. (S)	2–5	1–2	1–3	3–5	2–4	–	2–4
Jet Resolution (S)	4–7	1–3	1–4	2–5	2–4	–	4–6
Jet Energy Scale (S)	4–7	2–5	2–5	2–5	2–4	–	2–5
Vertex Conf. Jet (S)	4–10	5–12	4–10	7–10	5–10	–	4–8
$b$ -tag/taggability (S)	1–4	1–2	3–7	3–5	1–2	–	1–2
Heavy-Flavor K-factor	–	20	–	–	–	–	–
Inst.-WH $e\nu b\bar{b}$ (S)	1–2	2–4	1–3	1–2	1–3	15	1–2
Inst.-WH $\mu\nu b\bar{b}$	–	2.4	2.4	–	–	20	–
Cross Section	6	9	9	10	10	–	6.1
Signal Branching Fraction	–	–	–	–	–	–	1-9
ALPGEN MLM pos/neg(S)	–	SH	–	–	–	–	–
ALPGEN Scale (S)	–	SH	SH	–	–	–	–
Underlying Event (S)	–	SH	–	–	–	–	–
PDF, reweighting	2	2	2	2	2	–	2

$WH \rightarrow \ell\nu b\bar{b}$  Double Tag (DT) channels relative uncertainties (%)

Contribution	Dibosons	$W + b\bar{b}/c\bar{c}$	$W+l.f.$	$t\bar{t}$	single top	Multijet	$WH$
Luminosity	6.1	6.1	6.1	6.1	6.1	–	6.1
Electron ID/Trigger eff. (S)	2–5	2–3	2–3	1–2	1–2	–	1–2
Muon Trigger eff. (S)	2–4	1–2	1–2	2–4	1–3	–	2–5
Muon ID/Reco eff./resol.	4.1	4.1	4.1	4.1	4.1	–	4.1
Jet ID/Reco eff. (S)	2–8	2–5	4–9	3–7	2–4	–	3–7
Jet Resolution (S)	4–7	2–7	2–7	2–9	2–4	–	4–6
Jet Energy Scale (S)	4–7	2–6	2–7	2–6	2–7	–	4–6
Vertex Conf. Jet (S)	4–10	5–12	4–10	7–10	5–10	–	4–6
$b$ -tag/taggability (S)	3–7	4–6	3–10	5–10	4–10	–	4–9
Heavy-Flavor K-factor	–	20	–	–	–	–	–
Inst.-WH $e\nu b\bar{b}$ (S)	1–2	2–4	1–3	1–2	1–3	15	1–2
Inst.-WH $\mu\nu b\bar{b}$	–	2.4	2.4	–	–	20	–
Cross Section	6	9	9	10	10	–	6.1
Signal Branching Fraction	–	–	–	–	–	–	1-9
ALPGEN MLM pos/neg(S)	–	SH	–	–	–	–	–
ALPGEN Scale (S)	–	SH	SH	–	–	–	–
Underlying Event (S)	–	SH	–	–	–	–	–
PDF, reweighting	2	2	2	2	2	–	2

in Table XIII. The LLR distributions for the full combination are shown in Fig. 9. Included in these figures are the median LLR values for the signal-plus-background hypothesis ( $LLR_{s+b}$ ), background-only hypothesis ( $LLR_b$ ), and the observed data ( $LLR_{obs}$ ). The shaded bands represent the 1 and 2 standard deviation ( $\sigma$ ) departures for  $LLR_b$ . These distributions can be interpreted as follows:

- The separation between  $LLR_b$  and  $LLR_{s+b}$  provides a measure of the discriminating power of the search. This is the ability of the analysis to separate the  $s + b$  and  $b$ -only hypotheses.

TABLE IV: Systematic uncertainty ranges on the signal and background contributions and the error on the total background for the  $ZH \rightarrow \nu\nu b\bar{b}$  single (ST) and double tag (DT) channels. Systematic uncertainties are listed by name, see the original references for a detailed explanation of their meaning and on how they are derived. Systematic uncertainties for  $VH$  ( $WH+ZH$ ) shown in this table are obtained for  $m_H = 115 \text{ GeV}/c^2$ . Uncertainties are relative, in percent, and are symmetric unless otherwise indicated. Shape uncertainties are labeled with an “(S)”, and “SH” represents shape only uncertainty.

$ZH \rightarrow \nu\nu b\bar{b}$  Single Tag (ST) channels relative uncertainties (%)

Contribution	Top	$V + b\bar{b}/c\bar{c}$	$V+l.f.$	Dibosons	Total Bkgd	$VH$
Jet ID/Reco Eff (S)	2.0	2.0	2.0	2.0	1.9	2.0
Jet Energy Scale (S)	2.2	1.6	3.1	1.0	2.5	0.5
Jet Resolution (S)	0.5	0.3	0.3	0.9	0.3	0.8
Vertex Conf. / Taggability (S)	3.2	1.9	1.7	1.8	1.7	1.6
b Tagging (S)	1.1	0.8	1.8	1.2	1.3	3.2
Lepton Identification	1.6	0.9	0.8	1.0	0.8	1.1
Trigger	2.0	2.0	2.0	2.0	1.9	2.0
Heavy Flavor Fractions	–	20.0	–	–	4.1	–
Cross Sections	10.0	10.2	10.2	7.0	9.8	6.1
Signal Branching Fraction	–	–	–	–	–	1-9
Luminosity	6.1	6.1	6.1	6.1	5.8	6.1
Multijet Normalization	–	–	–	–	1.3	–
ALPGEN MLM (S)	–	–	SH	–	–	–
ALPGEN Scale (S)	–	SH	SH	–	–	–
Underlying Event (S)	–	SH	SH	–	–	–
PDF, reweighting (S)	SH	SH	SH	SH	SH	SH
Total uncertainty	12.8	23.6	12.9	10.1	12.3	9.8

$ZH \rightarrow \nu\nu b\bar{b}$  Double Tag (DT) channels relative uncertainties (%)

Contribution	Top	$V + b\bar{b}/c\bar{c}$	$V+l.f.$	Dibosons	Total Bkgd	$VH$
Jet ID/Reco Eff	2.0	2.0	2.0	2.0	1.9	2.0
Jet Energy Scale	2.1	1.6	3.4	1.2	2.2	0.2
Jet Resolution	0.7	0.4	0.5	1.5	0.5	0.7
Vertex Conf. / Taggability	2.6	1.6	1.6	1.8	1.7	1.4
b Tagging	6.2	4.3	4.3	3.7	3.6	5.8
Lepton Identification	2.0	0.9	0.8	0.9	1.0	1.1
Trigger	2.0	2.0	2.0	2.0	1.9	2.0
Heavy Flavor Fractions	–	20.0	–	–	8.0	–
Cross Sections	10.0	10.2	10.2	7.0	9.8	6.1
Signal Branching Fraction	–	–	–	–	–	1-9
Luminosity	6.1	6.1	6.1	6.1	5.8	6.1
Multijet Normalization	–	–	–	–	1.0	–
ALPGEN MLM pos/neg (S)	–	–	SH	–	–	–
ALPGEN Scale (S)	–	SH	SH	–	–	–
Underlying Event (S)	–	SH	SH	–	–	–
PDF, reweighting (S)	SH	SH	SH	SH	SH	SH
Total uncertainty	14.1	24.0	13.5	10.7	13.9	10.9

- The width of the  $LLR_b$  distribution (shown here as one and two standard deviation ( $\sigma$ ) bands) provides an estimate of how sensitive the analysis is to a signal-like background fluctuation in the data, taking account of the presence of systematic uncertainties. For example, the analysis sensitivity is limited when a  $1\sigma$  background fluctuation is large compared to the signal expectation.
- The value of  $LLR_{obs}$  relative to  $LLR_{s+b}$  and  $LLR_b$  indicates whether the data distribution appears to be more like signal-plus-background or background-only. As noted above, the significance of any departures of  $LLR_{obs}$  from  $LLR_b$  can be evaluated by the width of the  $LLR_b$  distribution.

Figure 10 illustrates the exclusion criterion  $1 - CL_s$  for the region  $100 \leq m_H \leq 200 \text{ GeV}/c^2$ . In addition, we provide in Fig. 11 the values for the observed  $1 - CL_{s+b}$  and its expected distribution as a function of  $m_H$ . The value  $CL_{s+b}$  is

TABLE V: Systematic uncertainties on the contributions for D0’s  $ZH \rightarrow \ell^+ \ell^- b\bar{b}$  channels. Systematic uncertainties are listed by name; see the original references for a detailed explanation of their meaning and on how they are derived. Systematic uncertainties for  $ZH$  shown in this table are obtained for  $m_H = 115 \text{ GeV}/c^2$ . Uncertainties are relative, in percent, and are symmetric unless otherwise indicated. Shape uncertainties are labeled with an “(S)”.

Contribution	$ZH$	Multijet	$Z+l.f.$	$Z+b\bar{b}$	$Z+c\bar{c}$	Dibosons	Top
Jet Energy Scale (S)	1.5	–	3.0	8.4	10	3.3	1.5
Jet Energy Resolution (S)	0.3	–	3.9	5.2	5.3	0.04	0.6
Jet ID (S)	0.6	–	0.9	0.6	0.2	1.0	0.3
Taggability (S)	5.1	–	5.2	7.2	7.3	6.9	6.5
$Z_{p_T}$ Model (S)	–	–	2.7	1.4	1.5	–	–
HF Tagging Efficiency (S)	4.9	–	–	5.0	9.4	–	5.2
LF Tagging Efficiency (S)	–	–	73	–	–	5.8	–
$ee$ Multijet Shape (S)	–	53	–	–	–	–	–
Multijet Normalization	–	20-50	–	–	–	–	–
$Z$ +jets Jet Angles (S)	–	–	1.7	2.7	2.8	–	–
Alpgen MLM (S)	–	–	0.3	–	–	–	–
Alpgen Scale (S)	–	–	0.4	0.2	0.2	–	–
Underlying Event (S)	–	–	0.2	0.05	0.08	–	–
Trigger (S)	0.4	–	0.03	0.2	0.3	0.3	0.4
Cross Sections	6.1	–	–	20	20	7	10
Signal Branching Fraction	1-9	–	–	–	–	–	–
Normalization	8	–	1.3	1.3	1.3	8	8
PDFs	0.55	–	1	2.4	1.1	0.66	5.9

Contribution	$ZH$	Multijet	$Z+l.f.$	$Z+b\bar{b}$	$Z+c\bar{c}$	Dibosons	Top
Jet Energy Scale (S)	2.3	–	4.0	6.4	8.2	3.8	2.7
Jet Energy Resolution(S)	0.6	–	2.6	3.9	4.1	0.9	1.5
JET ID (S)	0.8	–	0.7	0.3	0.2	0.7	0.4
Taggability (S)	3.6	–	8.6	6.5	8.2	4.6	2.1
$Z_{p_T}$ Model (S)	–	–	1.6	1.3	1.4	–	–
HF Tagging Efficiency (S)	0.8	–	–	1.3	3.2	–	0.7
LF Tagging Efficiency (S)	–	–	72	–	–	4.0	–
$ee$ Multijet Shape (S)	–	59	–	–	–	–	–
Multijet Normalization	–	20-50	–	–	–	–	–
$Z$ +jets Jet Angles (S)	–	–	2.0	1.5	1.5	–	–
Alpgen MLM (S)	–	–	0.4	–	–	–	–
Alpgen Scale (S)	–	–	0.2	0.2	0.2	–	–
Underlying Event(S)	–	–	0.07	0.02	0.1	–	–
Trigger (S)	0.4	–	0.3	0.2	0.1	0.2	0.5
Cross Sections	6.1	–	–	20	20	7	10
Signal Branching Fraction	1-9	–	–	–	–	–	–
Normalization	8	–	1.3	1.3	1.3	8	8
PDFs	0.55	–	1	2.4	1.1	0.66	5.9

the  $p$ -value for the signal-plus-background hypothesis. These values can be used as an alternative to the  $CL_s$  method to obtain upper limits. The  $CL_s = CL_{s+b}/CL_b$  formulation is intended to avoid setting limits when the background model grossly over-predicts the data or the data exhibit a large background-like fluctuation, as the value of  $CL_b$  will approach zero and the  $CL_s$  metric thus asymptotically limits the power of the search in such cases.

TABLE VI: Systematic uncertainties on the signal and background contributions for the  $H \rightarrow W^+W^- \rightarrow \ell^\pm \ell^\mp$  channels. Systematic uncertainties are listed by name; see the original references for a detailed explanation of their meaning and on how they are derived. Shape uncertainties are labeled with the ‘‘s’’ designation. Systematic uncertainties given in this table are obtained for the  $m_H = 165 \text{ GeV}/c^2$  Higgs selection. Cross section uncertainties on the  $gg \rightarrow H$  signal depend on the jet multiplicity, as described in the main text. Uncertainties are relative, in percent, and are symmetric unless otherwise indicated.

$H \rightarrow W^+W^- \rightarrow \ell^\pm \ell^\mp$  channels relative uncertainties (%)

Contribution	Dibosons	$Z/\gamma^* \rightarrow \ell\ell$	$W + \text{jet}/\gamma$	$t\bar{t}$	Multijet	$gg \rightarrow H$	$qq \rightarrow qqH$	$VH$
Luminosity/Normalization	6	6	6	6	30	6	6	6
Cross Section (Scale/PDF)	7-8	5	6	10	–	13-33/7.6-30	4.9	6.1
Signal Branching Fraction	–	–	–	–	–	0-7.3	0-7.3	0-7.3
PDF	2.5	2.5	2.5	2.5	–	8-30	8-30	8-30
Electron Identification	2.5	2.5	2.5	2.5	–	2.5	2.5	2.5
Muon Identification	4	4	4	4	–	4	4	4
Vertex Confirmation (s)	2-6	1-7	1-6	1-8	–	1-8	1-8	1-8
Jet identification (s)	2-5	2-5	2-5	2-5	–	2-5	2-5	2-5
Jet Energy Scale (s)	2-3	1-4	1-8	1-4	–	1-10	1-10	1-10
Jet Energy Resolution(s)	1-4	1-4	1-12	1-3	–	1-12	1-12	1-12
B-tagging	10	10	10	5	–	10	10	10

TABLE VII: Systematic uncertainties on the signal and background contributions for the  $H \rightarrow W^+W^- \rightarrow \mu\nu\tau_{had}\nu$  channel. Systematic uncertainties are listed by name; see the original references for a detailed explanation of their meaning and on how they are derived. Shape uncertainties are labeled with the shape designation (s). Systematic uncertainties shown in this table are obtained for the  $m_H = 165 \text{ GeV}/c^2$  Higgs selection. Uncertainties are relative, in percent, and are symmetric unless otherwise indicated.

$H \rightarrow W^+W^- \rightarrow \mu\nu\tau_{had}\nu$  channels relative uncertainties (%)

Contribution	Dibosons	$Z/\gamma^* \rightarrow \ell\ell$	$W + \text{jets}$	$t\bar{t}$	Multijet	$gg \rightarrow H$	$qq \rightarrow qqH$	$VH$
Luminosity ( $\sigma_{\text{inel}}(pp)$ )	4.6	4.6	–	4.6	–	4.6	4.6	4.6
Luminosity Monitor	4.1	4.1	–	4.1	–	4.1	4.1	4.1
Trigger	5.0	5.0	–	5.0	–	5.0	5.0	5.0
Lepton ID	3.7	3.7	–	3.7	–	3.7	3.7	3.7
Electron veto	5.0	–	–	5.0	–	5.0	5.0	5.0
Tau Energy Scale (s)	1.0	1.1	–	<1	–	<1	<1	<1
Jet Energy Scale (s)	8.0	<1	–	1.8	–	2.5	2.5	2.5
Jet identification (s)	<1	<1	–	7.5	–	5.0	5.0	5.0
Multijet (s)	–	–	–	–	20-50	–	–	–
Cross Section (Scale/PDF)	7.0	4.0	–	10	–	7/7.6	4.9	6.1
Signal Branching Fraction	–	–	–	–	–	0-7.3	0-7.3	0-7.3
Modeling	1.0	–	10	–	–	3.0	3.0	3.0

## V. CONCLUSIONS

We have presented upper limits on standard model Higgs boson production derived from 40 Higgs search analyses including data corresponding to  $4.3 - 8.6 \text{ fb}^{-1}$  (See Table I). We have combined these analyses and form new limits more sensitive than each individual limit. The observed 95% C.L. upper limits are found to be a factor of 1.83 (0.71) times the predicted standard model cross section at  $m_H = 115(165) \text{ GeV}/c^2$ , while the expected limit is found to be a factor of 1.90 (0.87) times the standard model prediction for the same mass. We exclude at the 95% C.L. the region  $161 < m_H < 170 \text{ GeV}/c^2$  with an *a priori* expected exclusion of  $159 < m_H < 170 \text{ GeV}/c^2$ . We are also becoming sensitive to the low mass region where we exclude with 95% C.L. the region  $100 < m_H < 105 \text{ GeV}/c^2$ , in agreement with the LEP exclusion.

TABLE VIII: Systematic uncertainties on the signal and background contributions for the  $H \rightarrow W^+W^- \rightarrow \ell\nu q\bar{q}$  electron and muon channels. Systematic uncertainties are listed by name; see the original references for a detailed explanation of their meaning and on how they are derived. Signal uncertainties are given for  $m_H = 160 \text{ GeV}/c^2$  for all channels. Cross section uncertainties on the  $gg \rightarrow H$  signal depend on the jet multiplicity, as described in the main text. Shape uncertainties are labeled with an “(S)”, and “SH” represents shape only uncertainty.

$H \rightarrow W^+W^- \rightarrow \ell\nu q\bar{q}$ Run II channels relative uncertainties (%)						
Contribution	$W$ +jets	$Z$ +jets	Top	Dibosons	$gg \rightarrow H$	$qq \rightarrow qqH$
Jet energy scale (S)	SH	< 0.1	$\pm 0.7$	$\pm 3.3$	$\binom{+5.7}{-4.0}$	$\pm 1.5$
Jet identification (S)	SH	< 0.1	$\pm 0.5$	$\pm 3.8$	$\pm 1.0$	$\pm 1.1$
Jet resolution (S)	SH	< 0.1	$\pm 0.5$	$\binom{+1.0}{-0.5}$	$\binom{+3.0}{-0.5}$	$\pm 0.8$
Association of jets with PV (S)	SH	SH	$\pm 1.2$	$\pm 3.2$	$\pm 2.9$	$\pm 2.4$
Luminosity	–	–	$\pm 6.1$	$\pm 6.1$	$\pm 6.1$	$\pm 6.1$
Muon trigger (S)	SH	< 0.1	< 0.1	< 0.1	< 0.1	< 0.1
Electron identification	$\pm 4.0$	$\pm 4.0$	$\pm 4.0$	$\pm 4.0$	$\pm 4.0$	$\pm 4.0$
Muon identification	$\pm 4.0$	$\pm 4.0$	$\pm 4.0$	$\pm 4.0$	$\pm 4.0$	$\pm 4.0$
ALPGEN tuning (S)	SH	SH	–	–	–	–
Cross Section (Scale/PDF)	$\pm 7$	$\pm 7$	$\pm 10$	$\pm 7$	$\pm 7/7.6$	$\pm 4.9$
Signal Branching Fraction	–	–	–	–	0-7.3	0-7.3
Heavy-flavor fraction (S)	$\pm 20$	$\pm 20$	–	–	–	–
PDF (S)	SH	SH	SH	SH	SH	SH
Multijet Background (S)		Electron channel $\pm 6.5$		Muon channel $\pm 26$		

TABLE IX: Systematic uncertainties on the signal and background contributions for  $VH \rightarrow VW\bar{W} \rightarrow \ell'^{\pm}\ell'^{\pm} + X$  channel. Systematic uncertainties are listed by name; see the original references for a detailed explanation of their meaning and on how they are derived. Shape only uncertainties are labeled with the “SH” designation. Systematic uncertainties for signal shown in this table are obtained for  $m_H = 160 \text{ GeV}/c^2$ . Uncertainties are relative, in percent, and are symmetric unless otherwise indicated.

$VH \rightarrow \ell^{\pm}\ell'^{\pm} + X$ Run IIa channel relative uncertainties (%)					
Contribution	Dibosons	$W$ +jet	Charge Flip	Multijet	$VH$
Cross section	7	6	–	–	6.1
Signal Branching Fraction	–	–	–	–	0-7.3
Normalization	4.7	4.7	–	–	4.7
JetID/JES	2	2	–	–	2
Jet-Lepton Fake	–	17-26	–	–	–
Instrumental ( $ee$ )	–	–	30	42	–
Instrumental ( $e\mu$ )	–	–	–	28	–
Instrumental ( $\mu\mu$ )	–	–	27	42	–
Instrumental Model	–	–	SH	SH	–
$VH \rightarrow \ell^{\pm}\ell'^{\pm} + X$ Run IIb channel relative uncertainties (%)					
Contribution	Dibosons	$W$ +jet	Charge Flip	Multijet	$VH$
Cross section	7	6	–	–	6.1
Signal Branching Fraction	–	–	–	–	0-7.3
Normalization	4.7	4.7	–	–	4.7
JetID/JES	2	2	–	–	2
Jet-Lepton Fake	–	20-32	–	–	–
Instrumental ( $ee$ )	–	–	15	30	–
Instrumental ( $e\mu$ )	–	–	–	18	–
Instrumental ( $\mu\mu$ )	–	–	11	29	–
Instrumental Model	–	–	SH	SH	–

TABLE X: Systematic uncertainties on the signal and background contributions for the  $\tau\tau jj$  Run IIb channel. Systematic uncertainties for the Higgs signal shown in this table are obtained for  $m_H = 135 \text{ GeV}/c^2$ . Systematic uncertainties are listed by name; see the original references for a detailed explanation of their meaning and on how they are derived. Uncertainties are relative, in percent, and are symmetric unless otherwise indicated. Shape uncertainties are labeled with an “(S).”

$\mu\tau_{had}jj$ Run IIb channel relative uncertainties (%)								
Contribution	$VH$	$q\bar{q} \rightarrow q\bar{q}H$	$gg \rightarrow H$	$W$ +jets	$Z$ +jets	Top	Dibosons	Multijet
Luminosity	6.1	6.1	6.1	6.1	6.1	6.1	6.1	–
$\mu$ ID	2.9	2.9	2.9	2.9	2.9	2.9	2.9	–
$\mu$ trigger	8.6	8.6	8.6	8.6	8.6	8.6	8.6	–
$\tau$ energy correction	9.8	9.8	9.8	9.8	9.8	9.8	9.8	–
$\tau$ track efficiency	1.4	1.4	1.4	1.4	1.4	1.4	1.4	–
$\tau$ selection by type	12,4,2,7	12,4,2,7	12,4,2,7	12,4,2,7	12,4,2,7	12,4,2,7	12,4,2,7	–
Cross section	6.1	4.9	33	6.0	6.0	10.0	7.0	–
GGF Signal PDF	–	–	29	–	–	–	–	–
GGF $H_{pT}$ Reweighting (S)	1.0	1.0	1.0	1.0	1.0	1.0	1.0	–
Vertex confirmation for jets	4.0	4.0	4.0	4.0	4.0	4.0	4.0	–
Jet ID(S)	$\sim 10$	$\sim 10$	$\sim 10$	$\sim 10$	$\sim 10$	$\sim 10$	$\sim 10$	–
Jet Energy Resolution (S)	$\sim 10$	$\sim 10$	$\sim 10$	$\sim 10$	$\sim 10$	$\sim 10$	$\sim 10$	–
Jet energy Scale (S)	$\sim 15$	$\sim 15$	$\sim 15$	$\sim 15$	$\sim 15$	$\sim 15$	$\sim 15$	–
Jet pT	5.5	5.5	5.5	5.5	5.5	5.5	5.5	–
PDF reweighting	2	2	2	2	2	2	2	–
Multijet Normalization	–	–	–	–	–	–	–	5.3
Multijet Shape	–	–	–	–	–	–	–	$\sim 15$

$e\tau_{had}jj$ Run IIb relative uncertainties (%)								
Contribution	$VH$	$q\bar{q} \rightarrow q\bar{q}H$	$gg \rightarrow H$	$W$ +jets	$Z$ +jets	Top	Dibosons	Multijet
Luminosity	6.1	6.1	6.1	6.1	6.1	6.1	6.1	–
Electron ID	4	4	4	4	4	4	4	–
Electron trigger	2	2	2	2	2	2	2	–
$\tau$ energy correction	9.8	9.8	9.8	9.8	9.8	9.8	9.8	–
$\tau$ track efficiency	1.4	1.4	1.4	1.4	1.4	1.4	1.4	–
$\tau$ selection by type	12,4,2,7	12,4,2,7	12,4,2,7	12,4,2,7	12,4,2,7	12,4,2,7	12,4,2,7	–
Cross section	6.1	4.9	33	6.0	6.0	10.0	7.0	–
GGF Signal PDF	–	–	29	–	–	–	–	–
GGF $H_{pT}$ Reweighting (S)	1.0	1.0	1.0	1.0	1.0	1.0	1.0	–
Signal Branching Fraction	0-7.3	0-7.3	0-7.3	–	–	–	–	–
Vertex confirmation for jets	4.0	4.0	4.0	4.0	4.0	4.0	4.0	–
Jet ID(S)	$\sim 10$	$\sim 10$	$\sim 10$	$\sim 10$	$\sim 10$	$\sim 10$	$\sim 10$	–
Jet Energy Resolution (S)	$\sim 10$	$\sim 10$	$\sim 10$	$\sim 10$	$\sim 10$	$\sim 10$	$\sim 10$	–
Jet energy Scale (S)	$\sim 15$	$\sim 15$	$\sim 15$	$\sim 15$	$\sim 15$	$\sim 15$	$\sim 15$	–
Jet pT	5.5	5.5	5.5	5.5	5.5	5.5	5.5	–
PDF reweighting	2	2	2	2	2	2	2	–
Multijet Normalization	–	–	–	–	–	–	–	4.7
Multijet Shape	–	–	–	–	–	–	–	$\sim 15$

### Acknowledgments

We thank the staffs at Fermilab and collaborating institutions, and acknowledge support from the DOE and NSF (USA); CEA and CNRS/IN2P3 (France); FASI, Rosatom and RFBR (Russia); CNPq, FAPERJ, FAPESP and FUNDUNESP (Brazil); DAE and DST (India); Colciencias (Colombia); CONACyT (Mexico); KRF and KOSEF (Korea); CONICET and UBACyT (Argentina); FOM (The Netherlands); STFC and the Royal Society (United Kingdom); MSMT and GACR (Czech Republic); CRC Program and NSERC (Canada); BMBF and DFG (Germany); SFI (Ireland); The Swedish Research Council (Sweden); and CAS and CNSF (China).

TABLE XI: Systematic uncertainties on the signal and background contributions for the  $H \rightarrow \gamma\gamma$  channel. Systematic uncertainties for the Higgs signal shown in this table are obtained for  $m_H = 125 \text{ GeV}/c^2$ . Systematic uncertainties are listed by name; see the original references for a detailed explanation of their meaning and on how they are derived. Uncertainties are relative, in percent, and are symmetric unless otherwise indicated.

$H \rightarrow \gamma\gamma$  channel relative uncertainties (%)

Contribution	Background	$gg \rightarrow H$
Luminosity	6.1	6.1
Acceptance	–	2
electron ID efficiency	2	–
electron track-match inefficiency	10	–
Photon ID efficiency	3	3
Photon energy scale	2	1
Cross Section (Scale/PDF)	4	7/7.6
Background subtraction	15	–

TABLE XII: The correlation matrix for the analysis channels. All uncertainties within a group are considered 100% correlated across channels. The correlated systematic uncertainty on the background cross section ( $\sigma$ ) is itself subdivided according to the different background processes in each analysis.

Source	$WH \rightarrow \ell\nu b\bar{b}$	$ZH \rightarrow \nu\bar{\nu} b\bar{b}$	$ZH \rightarrow \ell\ell b\bar{b}$	$H \rightarrow W^+W^- \rightarrow \ell^\pm\nu\ell^\mp\nu$
Luminosity	×	×		
Normalization				
Jet Energy Scale	×	×	×	×
Jet ID	×	×	×	×
Tau Energy Scale/ID				
Electron ID/Trigger	×	×	×	×
Muon ID/Trigger	×	×	×	×
Photon ID/Trigger				
$b$ -Jet Tagging	×	×	×	
Background $\sigma$	×	×	×	×
Background Modeling				
Multijet				
Signal $\sigma$	×	×	×	×
Signal modeling				×

Source	$H+X \rightarrow \mu^\pm\tau_{had}^\mp + \leq 1j$	$H+X \rightarrow \ell^\pm\tau_{had}^\mp jj$	$H \rightarrow W^+W^- \rightarrow \ell\nu q\bar{q}$	$VH \rightarrow \ell^\pm\ell^\pm + X$	$H \rightarrow \gamma\gamma$
Luminosity	×	×	×		×
Normalization					
Jet Energy Scale	×	×	×	×	
Jet ID	×	×	×	×	
Tau Energy Scale/ID	×	×			
Electron ID/Trigger	×	×	×	×	
Muon ID/Trigger	×	×	×	×	
Photon ID/Trigger					×
$b$ -Jet Tagging					
Background $\sigma$	×	×	×	×	
Background Modeling					
Multijet					
Signal $\sigma$	×	×	×	×	×
Signal modeling	×	×	×	×	×

TABLE XIII: Combined 95% C.L. limits on  $\sigma \times BR(H \rightarrow X)$  for SM Higgs boson production. The limits are reported in units of the SM production cross section times branching fraction.

$m_H$	100	105	110	115	120	125	130	135	140	145	150	155	160	165	170	175	180	185	190	195	200
Expected:	1.43	1.54	1.71	1.90	2.02	2.15	2.14	1.98	1.79	1.63	1.42	1.22	0.92	0.87	1.01	1.18	1.42	1.79	2.17	2.54	2.95
Observed:	0.79	0.97	1.29	1.83	1.91	2.94	2.96	2.25	2.42	2.63	2.06	1.85	1.13	0.71	1.00	1.56	1.69	2.13	2.49	2.80	3.61

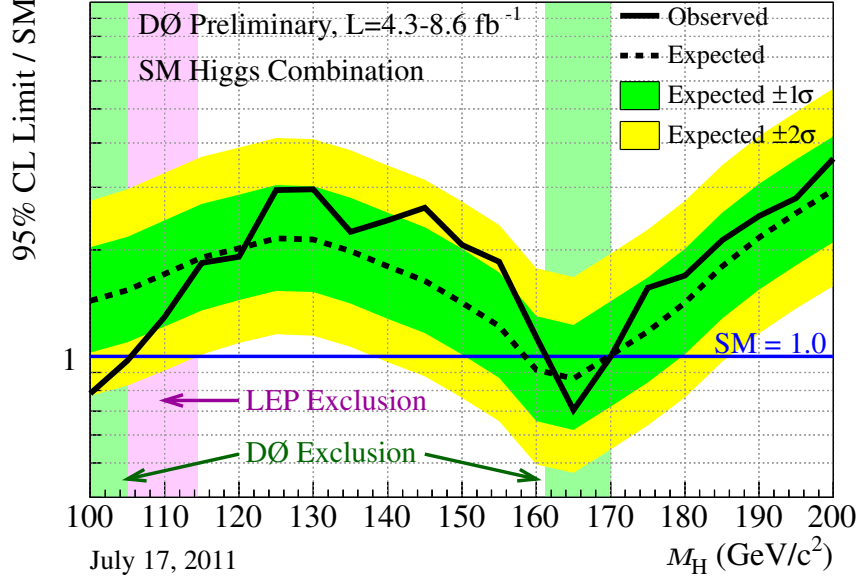


FIG. 8: Expected (median) and observed 95% C.L. cross section upper limit ratios for the combined  $WH/ZH/H, H \rightarrow b\bar{b}/W^+W^-/\gamma\gamma/\tau^+\tau^-$  analyses over the  $100 \leq m_H \leq 200$   $\text{GeV}/c^2$  mass range. The green and yellow bands correspond to the regions enclosing 1- $\sigma$  and 2- $\sigma$  fluctuations of the background, respectively.

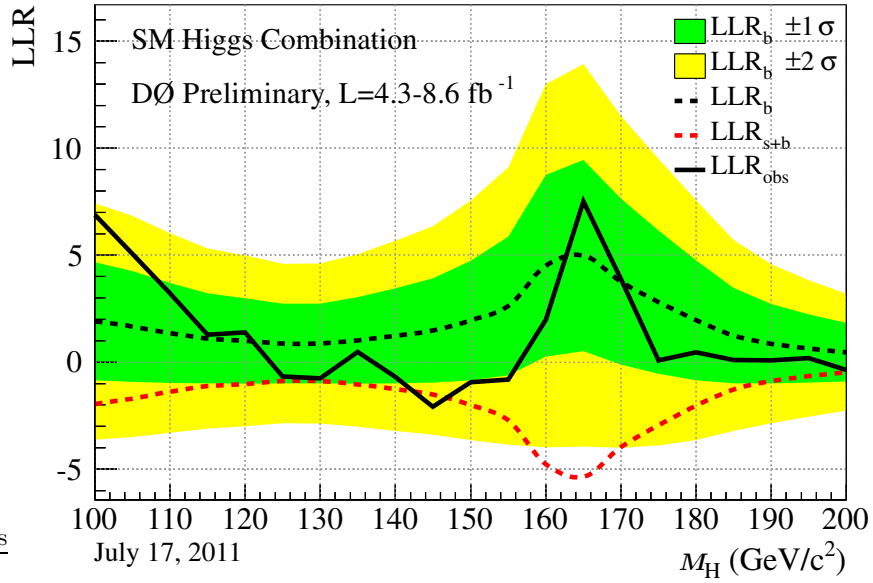


FIG. 9: Log-likelihood ratio distribution for the combined  $WH/ZH/H, H \rightarrow b\bar{b}/W^+W^-/\gamma\gamma/\tau^+\tau^-$  analyses over the  $100 \leq m_H \leq 200$   $\text{GeV}/c^2$  mass range. The green and yellow bands correspond to the regions enclosing 1- $\sigma$  and 2- $\sigma$  fluctuations of the background, respectively.

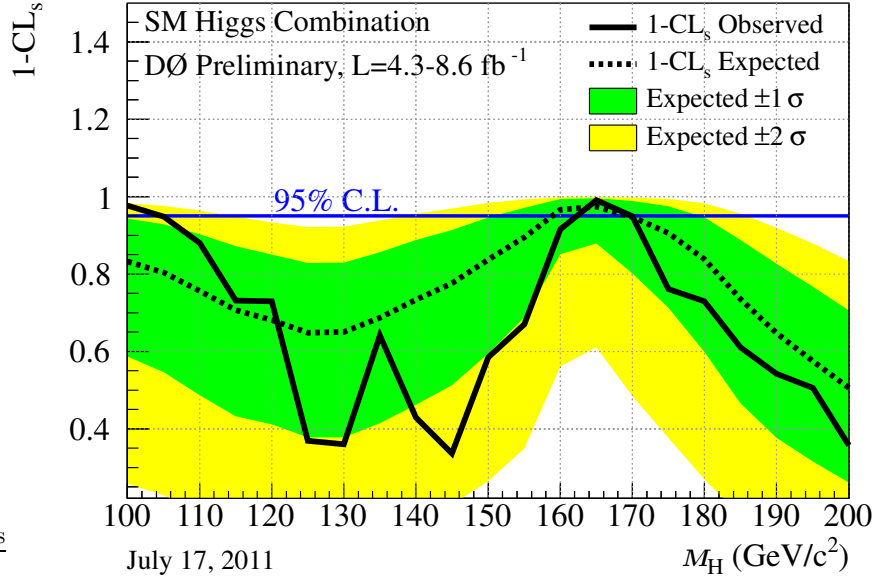


FIG. 10: The  $1 - CL_S$  (exclusion probability) distribution for the combined  $WH/ZH/H, H \rightarrow b\bar{b}/W^+W^-/\gamma\gamma/\tau^+\tau^-$  analyses over the  $100 \leq m_H \leq 200$   $\text{GeV}/c^2$  mass range. The green and yellow bands correspond to the regions enclosing  $1\text{-}\sigma$  and  $2\text{-}\sigma$  fluctuations of the background, respectively.

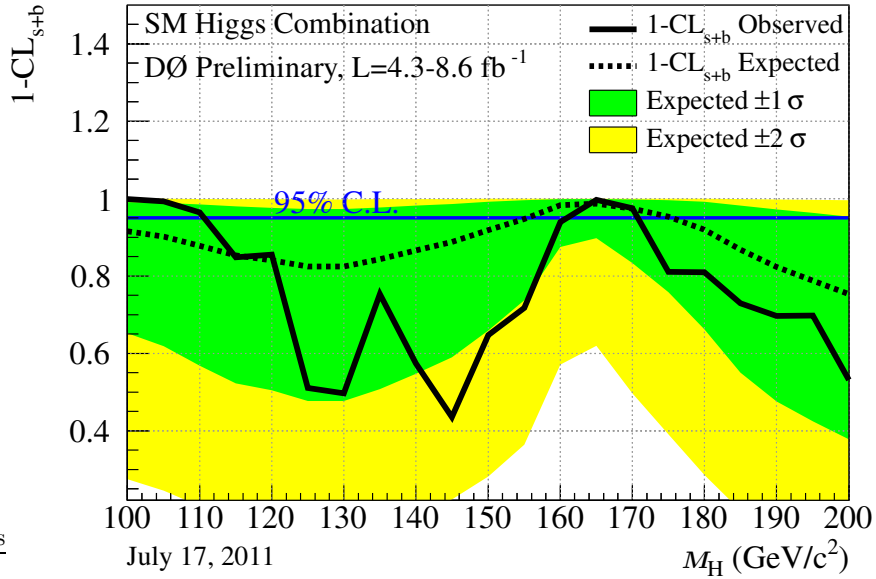


FIG. 11: The  $1 - CL_{S+b}$  (signal-plus-background  $p$ -value) distribution for the combined  $WH/ZH/H, H \rightarrow b\bar{b}/W^+W^-/\gamma\gamma/\tau^+\tau^-$  analyses over the  $100 \leq m_H \leq 200$   $\text{GeV}/c^2$  mass range. The green and yellow bands correspond to the regions enclosing  $1\text{-}\sigma$  and  $2\text{-}\sigma$  fluctuations of the background, respectively.

- 
- [1] R. Barate *et al.* [LEP Working Group for Higgs boson searches], Phys. Lett. B **565**, 61 (2003), [arXiv:hep-ex/0306033].
- [2] The LEP Electroweak Working Group, "Status of July 2010", <http://lepewwg.web.cern.ch/LEPEWWG/>.
- [3] DØ Collaboration, V. Abazov *et al.*, Nucl. Instrum. Meth. A **565**, 463 (2006) [arXiv:hep-ph/0507191].
- [4] DØ Collaboration, DØ Note 6220-CONF.
- [5] DØ Collaboration, DØ Note 6223-CONF.
- [6] DØ Collaboration, DØ Note 6166-CONF.
- [7] DØ Collaboration, DØ Note 6219-CONF.
- [8] DØ Collaboration, Phys. Rev. Lett. **106** (2011) 171802 [arXiv:1101.6079v2 [hep-ph]].
- [9] DØ Collaboration, DØ Note 6179-CONF.
- [10] DØ Collaboration, e-Print: arXiv:1107.1268v1 [hep-ph].
- [11] DØ Collaboration, DØ Note 6171-CONF.
- [12] DØ Collaboration, DØ Note 6177-CONF.
- [13] DØ Collaboration, V. Abazov *et al.*, Nucl. Instrum. Methods in Phys. Res. Sect. A **620**, 490 (2010) [arXiv:1002.4224].
- [14] DØ Collaboration, DØ Note 6094-CONF.
- [15] DØ Collaboration, DØ Note 6183-CONF.
- [16] T. Sjöstrand, L. Lonnblad and S. Mrenna, arXiv:hep-ph/0108264.
- [17] M. L. Mangano, M. Moretti, F. Piccinini, R. Pittau and A. D. Polosa, JHEP **0307**, 001 (2003). [arXiv:hep-ph/0206293].
- [18] A. Pukhov *et al.*, arXiv:hep-ph/9908288.
- [19] J. Campbell and R. K. Ellis, <http://mcfm.fnal.gov/>.  
J. M. Campbell, R. K. Ellis, Nucl. Phys. Proc. Suppl. **205-206**, 10-15 (2010). [arXiv:1007.3492 [hep-ph]].
- [20] The CDF and DØ Collaborations and the TEVNPHWG Working Group, "Combined CDF and DØ Upper Limits on Standard Model Higgs-Boson Production with up to 8.2 fb<sup>-1</sup> of Data", FERMILAB-CONF-11-044-E, CDF Note 10441, DØ Note 6184.  
The CDF and DØ Collaborations and the TEVNPHWG Working Group, "Combined CDF and DØ Upper Limits on Standard Model Higgs-Boson Production with up to 8.6 fb<sup>-1</sup> of Data", FERMILAB-CONF-11-XXX-E, CDF Note 10606, DØ Note 6226.
- [21] C. Anastasiou, R. Boughezal and F. Petriello, JHEP **0904**, 003 (2009).
- [22] D. de Florian and M. Grazzini, Phys. Lett. B **674**, 291 (2009).
- [23] M. Grazzini, private communication (2010).
- [24] The CDF and DØ Collaborations and the Tevatron Electroweak Working Group, arXiv:1007.3178 [hep-ex], arXiv:0903.2503 [hep-ex].
- [25] I. W. Stewart, F. J. Tackmann, [arXiv:1107.2117 [hep-ph]].
- [26] R. V. Harlander and W. B. Kilgore, Phys. Rev. Lett. **88**, 201801 (2002).
- [27] C. Anastasiou and K. Melnikov, Nucl. Phys. B **646**, 220 (2002).
- [28] V. Ravindran, J. Smith, and W. L. van Neerven, Nucl. Phys. B **665**, 325 (2003).
- [29] S. Actis, G. Passarino, C. Sturm, and S. Uccirati, Phys. Lett. B **670**, 12 (2008).
- [30] U. Aglietti, R. Bonciani, G. Degrossi, A. Vicini, arXiv:hep-ph/0610033v1 (2006).
- [31] S. Catani, D. de Florian, M. Grazzini and P. Nason, JHEP **0307**, 028 (2003) [arXiv:hep-ph/0306211].
- [32] A. D. Martin, W. J. Stirling, R. S. Thorne and G. Watt, Eur. Phys. J. C **63**, 189 (2009).
- [33] <http://www.hep.ucl.ac.uk/pdf4lhc/>;  
S. Alekhin *et al.*, (PDF4LHC Working Group), [arXiv:1101.0536v1 [hep-ph]];  
M. Botje *et al.*, (PDF4LHC Working Group), [arXiv:1101.0538v1 [hep-ph]].
- [34] P. M. Nadolsky *et al.*, Phys. Rev. D **78**, 013004 (2008) [arXiv:0802.0007 [hep-ph]].
- [35] R. D. Ball *et al.* [NNPDF Collaboration], Nucl. Phys. B **809**, 1 (2009) [Erratum-ibid. B **816**, 293 (2009)] [arXiv:0808.1231 [hep-ph]].
- [36] C. Anastasiou, G. Dissertori, M. Grazzini, F. Stöckli and B. R. Webber, JHEP **0908**, 099 (2009). [arXiv:0905.3529 [hep-ph]].
- [37] J. M. Campbell, R. K. Ellis, C. Williams, Phys. Rev. **D81**, 074023 (2010). [arXiv:1001.4495 [hep-ph]].
- [38] H. L. Lai *et al.*, Phys. Rev. D **55**, 1280 (1997).
- [39] G. Bozzi, S. Catani, D. de Florian, and M. Grazzini, Phys. Lett. B **564**, 65 (2003); // G. Bozzi, S. Catani, D. de Florian, and M. Grazzini, Nucl. Phys. B **737**, 73 (2006).
- [40] C. Balazs, J. Huston, I. Puljak, Phys. Rev. D **63** 014021 (2001).  
C. Balazs and C.-P. Yuan, Phys. Lett. B **478** 192-198 (2000).  
Qing-Hong Cao and Chuan-Ren Chen, Phys. Rev. D **76** 073006 (2007).
- [41] J. Baglio and A. Djouadi, JHEP **1010**, 064 (2010) [arXiv:1003.4266v2 [hep-ph]].
- [42] The Fortran program can be found on Michael Spira's web page <http://people.web.psi.ch/~mspira/proglist.html>.
- [43] O. Brein, A. Djouadi, and R. Harlander, Phys. Lett. B **579**, 149 (2004).
- [44] M. L. Ciccolini, S. Dittmaier, and M. Kramer, Phys. Rev. D **68**, 073003 (2003).
- [45] P. Bolzoni, F. Maltoni, S.-O. Moch, and M. Zaro, Phys. Rev. Lett. **105**, 011801 (2010) [arXiv:1003.4451v2 [hep-ph]].
- [46] M. Ciccolini, A. Denner, and S. Dittmaier, Phys. Rev. Lett. **99**, 161803 (2007) [arXiv:0707.0381 [hep-ph]];  
M. Ciccolini, A. Denner, and S. Dittmaier, Phys. Rev. D **77**, 013002 (2008) [arXiv:0710.4749 [hep-ph]].

We would like to thank the authors of the HAWK program for adapting it to the Tevatron.

- [47] A. Djouadi, J. Kalinowski and M. Spira, *Comput. Phys. Commun.* **108**, 56 (1998).
- [48] J. Baglio and A. Djouadi, arXiv:1012.0530 [hep-ph] (2010).
- [49] T. Junk, *Nucl. Instrum. Meth. A* **434**, 435 (1999); A.Read, CERN 2000-005 (30 May 2000).
- [50] T. Andeen *et al.*, Report No. FERMILAB-TM-2365, 2007.
- [51] W. Fisher, FERMILAB-TM-2386-E.